

Intrinsic Ferromagnetism in the Diluted Magnetic Semiconductor Co:TiO₂

H. Saadaoui,¹ X. Luo,² Z. Salman,¹ X. Y. Cui,³ N. N. Bao,⁴ P. Bao,⁵ R. K. Zheng,⁵ L. T. Tseng,² Y.H. Du,⁶ T. Prokscha,¹ A. Suter,¹ T. Liu,⁷ Y. R. Wang,² S. Li,² J. Ding,⁴ S. P. Ringer,^{3,8} E. Morenzoni,^{1,*} and J. B. Yi^{2,†}

¹Laboratory for Muon Spin Spectroscopy, Paul Scherrer Institute, 5232 Villigen, Switzerland

²School of Materials Science and Engineering, University of New South Wales, Kensington, New South Wales 2052, Australia

³School of Aerospace, Mechanical and Mechatronic Engineering,

The University of Sydney, Sydney, New South Wales 2006, Australia

⁴Department of Materials Science and Engineering,

National University of Singapore, 119260, Singapore

⁵School of Physics, The University of Sydney, Sydney, New South Wales 2006, Australia

⁶Institute of Chemical and Engineering Science, Agency for Science,

Technology and Research, 1 Pesek Road, Jurong Island, 627833, Singapore

⁷ANKA, Karlsruhe Institute of Technology, 76344 Eggenstein-Leopoldshafen, Germany

⁸The Australian Institute for Nanoscale Science and Technology,

The University of Sydney, Sydney, New South Wales 2006, Australia

(Dated: March 10, 2022)

Here we present a study of magnetism in Co_{0.05}Ti_{0.95}O_{2- δ} anatase films grown by pulsed laser deposition under a variety of oxygen partial pressures and deposition rates. Energy-dispersive spectrometry and transition electron microscopy analyses indicate that a high deposition rate leads to a homogeneous microstructure, while very low rate or postannealing results in cobalt clustering. Depth resolved low-energy muon spin rotation experiments show that films grown at a low oxygen partial pressure ($\approx 10^{-6}$ torr) with a uniform structure are fully magnetic, indicating intrinsic ferromagnetism. First principles calculations identify the beneficial role of low oxygen partial pressure in the realization of uniform carrier-mediated ferromagnetism. This work demonstrates that Co:TiO₂ is an intrinsic diluted magnetic semiconductor.

Diluted magnetic semiconductors (DMSs) have received intensive attention because of their potential applications in spintronics devices, which are based on novel concepts utilizing both the charge and spin of the electron. One challenging hurdle is achieving intrinsic ferromagnetism at room temperature. Oxide based DMSs are the most promising candidates owing to their possible high Curie temperature [1–6], compared to the III-V compound based DMSs, such as (Ga,Mn)As [7, 8]. However, reproducibility problems of oxide DMSs have been reported in several cases, where ferromagnetism is only apparent in samples prepared in a poor oxygen environment. Magnetic clusters and secondary phases have been shown to lead to extrinsic ferromagnetism in these systems [9–11]. Therefore, understanding the origin of ferromagnetism in oxide DMSs is still an object of intense debate [12, 13].

One of the most prominent systems is Co-doped TiO₂, the first reported oxide-based DMS with a Curie temperature T_C as high as 600 K [2]. Ferromagnetism can be induced in paramagnetic Co_xTi_{1-x}O_{2- δ} films with an electric field [4], suggesting that magnetism is carrier mediated. However, Co clustering in this system has been widely reported to cause room temperature ferromagnetism ($T_C = 1388$ K in Co) [11, 14]. Ferromagnetism can be also caused by nucleation of highly Co-enriched anatase nanoparticles [15] The discrepancy of these results has severely affected the development of DMS materials. Currently, there is no direct evidence of spatially uniform ferromagnetism as expected from carrier

mediation or Ruderman-Kittel-Kasuya-Yosida (RKKY) interaction. There is only evidence of localized structural uniformity by high resolution transmission electron microscopy (HRTEM)[4]. Therefore, a detailed investigation of the microscopic magnetic properties is required to identify the ideal growth conditions to achieve structural and intrinsic magnetic uniformity.

In this work, we use low-energy muon spin rotation spectroscopy (LE- μ SR) [16] as a local magnetic probe to examine the influence of growth conditions on the magnetism in Co-doped TiO₂ thin films deposited by pulsed laser deposition (PLD). We find spatially uniform and intrinsic ferromagnetism in Co_{0.05}Ti_{0.95}O_{2- δ} films deposited under an oxygen partial pressure $P_{O_2}=10^{-6}$ torr. The structure uniformity of the films is confirmed by x-ray diffraction (XRD) and HRTEM. The magnetic volume fraction and the internal field width decrease with increasing oxygen partial pressure. This work directly proves that an intrinsic DMS system can be synthesized with both structural and magnetic uniformity.

The films were deposited by PLD in various oxygen partial pressures with a laser pulse power of 1.8 J/cm², corresponding to a rate of 10 nm/min. The nominal thickness of the films is approximately 50 nm. The films are epitaxially grown in the anatase structure as confirmed by XRD. HRTEM imaging shows that films deposited under $P_{O_2}=10^{-5}$ and 10^{-6} torr have a homogeneous cluster-free microstructure (Fig.S2). Energy dispersive x-ray spectroscopy (EDX) mapping reveals that Ti, O, and Co atoms are uniformly distributed in films

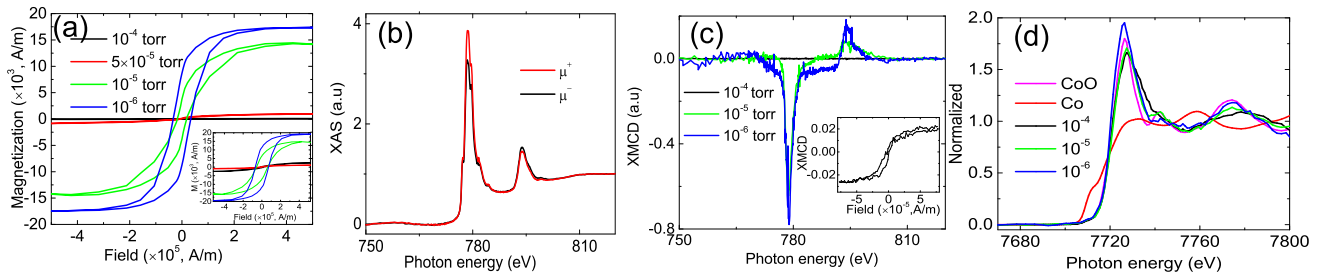


FIG. 1: (a) M-H loops at room temperature of films deposited under an oxygen partial pressure of 10^{-6} , 10^{-5} , 5×10^{-5} , and 10^{-4} torr. The inset shows the M-H loops at 5 K. (b) Co-L edge XAS spectra of the film deposited at 10^{-5} torr. (c) XMCD signal of the films deposited under 10^{-6} , 10^{-5} , and 10^{-4} torr. The inset shows the XMCD hysteresis of the Co-L edge in the sample grown at 10^{-5} torr. (d) Co-K edge XANES spectra

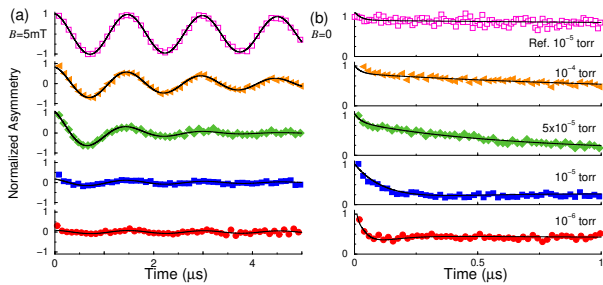


FIG. 2: The LE- μ SR spectra in $\text{Co}_{0.05}\text{Ti}_{0.95}\text{O}_{2-\delta}$ samples grown at different partial oxygen pressures. The spectra are normalized to the initial amplitude of the asymmetry of the reference sample (undoped TiO_2). (a) Asymmetry in a transverse field of $B = 5$ mT applied parallel to the sample surface, measured at 5 K. The initial amplitude at the different oxygen pressures is a measure of the paramagnetic fraction as explained in the text. (b) Typical asymmetry spectra in zero field. All solid lines are the fitted curves described in the supporting material.

grown at 10^{-5} and 10^{-6} torr. However, a nonuniform clustered microstructure has been observed in films deposited under 10^{-4} torr (Fig. S3 in the Supplemental Material [17]).

Figure 1(a) shows the hysteresis loops of the films deposited under different oxygen partial pressures. A deposition pressure of 10^{-5} and 10^{-6} torr leads to magnetic films at 300 K that clearly show hysteresis loops, while growth pressures of 10^{-4} and 5×10^{-5} torr lead to a negligible magnetic signal. Similar hysteresis loops are seen at 5 K (inset of Fig.1(a)) with a slight increase of saturation magnetization.

From the saturation magnetization, we estimate the Co magnetic moment to be $\sim 1.03 \mu_B$ in the 10^{-6} torr sample and $0.93 \mu_B$ in the 10^{-5} torr sample. Pure TiO_2 films deposited under $P_{\text{O}_2} = 10^{-5}$ torr show no ferromagnetism at all temperatures, indicating that oxygen vacancies or Ti^{3+} alone are not the origin of the ferromagnetism. A similar strong pressure dependence is seen in the carrier concentration as measured by the Hall effect. The

films deposited under $P_{\text{O}_2} = 5 \times 10^{-5}$, 10^{-5} , and 10^{-6} torr have carrier concentrations of 6.4×10^{17} , 2.1×10^{18} , and $2.0 \times 10^{19} \text{ cm}^{-3}$, respectively, whereas the film deposited under $P_{\text{O}_2} = 10^{-4}$ torr is insulating.

Figure 1(b) shows x-ray absorption spectroscopy (XAS) spectra at the Co L-edge of the film deposited under $P_{\text{O}_2} = 10^{-5}$ torr. The multiplet feature of XAS confirms the +2 valence state of Co. Figure 1(c) shows the x-ray magnetic circular dichroism XMCD signal in three films ($P_{\text{O}_2} = 10^{-4}$, 10^{-5} , and 10^{-6} torr) taken at 300 K. A strong signal is observed in the 10^{-5} and 10^{-6} torr samples, whereas no signal is observed in the film grown at 10^{-4} torr. No magnetic features are observed at the O and Ti edges, confirming that only Co substitution is the origin of the observed magnetization in the films. Using sum rules calculations [26], we estimate the magnetic moments of Co to be 0.95 and $0.81 \mu_B$, in the 10^{-6} and 10^{-5} torr samples respectively. These estimates are slightly lower than the values obtained from the magnetization measurements mentioned above, likely due to surface effects [27]. The inset shows the hysteresis of the XMCD signal, where the magnetization of Co saturates at about 0.2 T, confirming the ferromagnetic phase of the film. In order to confirm the Co ion valence state, we performed X-ray absorption near edge spectroscopy (XANES) measurements at the Co K-edge of the samples and compared the spectra with reference samples.[28] In all the samples Co show a 2+ state. Because of lower oxygen partial pressure, Co in the $P_{\text{O}_2} = 10^{-6}$ sample has a slightly lower valence state than in 10^{-4} and 10^{-5} . The spectra shown in Fig. 1(d) confirm the absence of metallic Co clusters.

HRTEM and EDX analysis can only give information about the structure uniformity and chemical composition. On the other hand, magnetization measurements by a SQUID give only a macroscopic, sample averaged information of the magnetic state. To determine the local magnetic properties and the magnetic volume fraction we use μ SR as a sensitive magnetic probe [29]. Fully polarized muons are implanted in the sample. The subsequent

precession and relaxation of their spins lead to a temporal evolution of the polarization, which is easily detectable via the asymmetric muon decay, and can be used to determine static and dynamic magnetic properties in the sample. To study the homogeneity of Co-TiO₂ thin films prepared by PLD, we use LE- μ SR which allows a depth dependent study on a nm scale [16]. This technique has been successfully applied to a variety of systems such as (Ga,Mn)As DMS [30] or oxide heterostructures [31–34].

We performed LE- μ SR measurements in a weak magnetic transverse field (TF) (5 mT) perpendicular to the substrate surface and the initial muon spin polarization. Typical spectra are shown in Fig. 2(a). This measurement allows to determine the magnetic volume fraction of the sample. In a paramagnetic environment the local field sensed by the muons is determined by the applied field and a weakly damped muon spin precession is observed. The undoped TiO₂ sample grown at $P_{O_2}=10^{-5}$ torr defines the reference showing the full asymmetry of a paramagnetic sample (A_{ref}). If part of the sample is magnetic muons stopping in that environment quickly depolarize since field and field width are much larger than the applied field and do not contribute to the precession component characteristic of the paramagnetic environment, whose amplitude A is therefore proportional to the paramagnetic fraction of the sample. Its dependence on P_{O_2} is therefore a direct measure of the evolution of the magnetic volume fraction under different preparation conditions (see the Supplemental Material for details of the data analysis). The reference spectrum is weakly damped, while all Co-doped samples are either more damped or have an initial amplitude lower than the full amplitude of the reference sample. The dependence of the paramagnetic volume fraction ($F_{pm} = \frac{A}{A_{ref}} \times 100\%$) on the partial pressure P_{O_2} is shown in Fig. 3. The paramagnetic volume fraction increases with oxygen partial pressure, where paramagnetism and ferromagnetism co-exist in the same sample. The film becomes paramagnetic for pressures $\gtrsim 5 \times 10^{-5}$ torr. The sample grown in 10^{-6} torr is almost fully magnetic with a paramagnetic fraction less than 5% (within the LE- μ SR experimental error), due mostly to the muons landing in the film-free edges of the substrate. Figure 3(a) shows the temperature dependence of the original TF- μ SR spectra without any normalization, indicating that there is almost no change for the spectra at 5, 100 and 200 K, confirming that the ferromagnetic ordering is not due to the clustering of dopants.

The film deposited under 10^{-4} torr has a $\sim 13\%$ ferromagnetic phase fraction at 5 K. As shown in Fig. 1(a), the film shows a slightly higher saturation magnetization at 5 K than that of the film deposited at $P_{O_2}=5 \times 10^{-5}$ torr. This residual ferromagnetic phase may be due to the formation of isolated magnetic polarons in an insulating state [35], which is supported by first principles density functional theory (DFT) calculations, as discussed

later.

The LE- μ SR measurements in zero field (ZF) are sensitive to the local magnetization, since the muon spin relaxation rate Δ is proportional to the width of the local field distribution. Typical asymmetry spectra taken at 5 K with 4 keV muons are shown in Fig. 2(b). At this energy the muon implantation profile with a mean stopping depth of 21.2 nm and a rms of 7.1 nm covers the central part of the film with thickness 50 nm (see Fig. S8 in the Supplemental Material). The samples grown at low pressures ($P_{O_2}=10^{-5}$ and 10^{-6} torr) do not show any spontaneous precession, as we would expect in the case of long range ferromagnetic order with well defined wave vector, but a rapid damping of the muon spin polarization, characteristic of the muons experiencing a very broad distribution of static fields, due to the random position of the muons with respect to the magnetic moments. The signal in the undoped reference sample is slowly relaxing typical of a nonmagnetic sample. The signal in the film grown at 10^{-4} torr sample shows a fast relaxation at early times with a small amplitude reflecting a $\approx 10\%$ fraction of clustered ferromagnetic phases and a dominant slowly relaxing component as expected in a paramagnetic state, while the sample grown at 5×10^{-5} shows a signal of intermediate relaxation between the weakly and strongly magnetic samples.

The width of the internal magnetic field Δ is shown in Fig. 3. It is weakly dependent on temperature but decreases strongly with increasing oxygen partial pressure. It is high at low pressure and approaches the limit of the paramagnetic reference sample in samples grown at pressures above 5×10^{-5} torr. From the ZF- and TF LE- μ SR measurements, we conclude that the film deposited under 10^{-6} torr shows spatially homogeneous ferromagnetism encompassing the full volume fraction and suggesting a uniform distribution of Co dopants. This ordering is mediated by itinerant carriers, since similar films deposited under a high oxygen partial pressure show weak or no ferromagnetism. Varying the implantation energy LE- μ SR allows us also to follow the magnetic properties as a function of depth on a nanometer scale [36]. We find the results only weakly dependent on the implantation depth, further confirming the homogeneous character of the ferromagnetism. No evidence of ferromagnetism is observed at the interface of undoped TiO₂ and the LaAlO₃ substrate, which was suggested to be one of the origins [37, 38].

The LE- μ SR and structure results rule out Co clustering as an extrinsic origin of ferromagnetism. We find that the rate of deposition influences the nature of the magnetic phase. Using HRTEM and EDX mapping we have observed Co clustering in films deposited under $P_{O_2}=10^{-6}$ torr with a low deposition rate (1 nm/min), or postannealed in vacuum under different oxygen partial pressures (Supplemental Material). This suggests that the relatively fast and nonequilibrium deposition at low

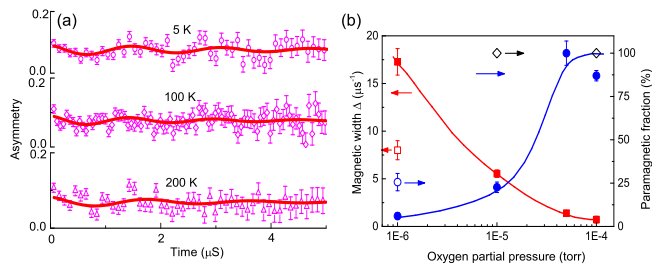


FIG. 3: (a) TF LE- μ SR spectra of Co-TiO₂ deposited under $P_{O_2}=10^{-6}$ torr at 5, 100 and 200 K. (b) The width of the internal magnetic field (Δ) (left y -axis) and the paramagnetic fraction (F_{pm}) (right y axis) versus the partial oxygen pressure during growth. Δ is found using the ZF spectra (Fig. 2-(b)). F_{pm} is extracted from the amplitude of the oscillating part of the asymmetry in TF (Fig. 2-(a)). The red open square and blue open circle respectively represent the internal field width and the paramagnetic fraction in the clustered film. Open black diamonds refer to the full paramagnetic volume fraction of the nondoped reference samples. The solid lines are guides to the eye.

P_{O_2} may be impeding the diffusion of oxygen vacancies leading to a uniform distribution of Co dopants [39]. In the clustered 10^{-6} film, the XMCD measurement shows a Co moment of $\sim 0.90 \mu_B$, slightly lower than $1.03 \mu_B$ measured in cluster-free sample. A larger difference is measured by the local muon probe. The LE- μ SR measurements show a smaller magnetic fraction of $\sim 75\%$ in the clustered film and a field width Δ that is about half of that in the strongly magnetic samples (see open symbols in Fig. 3). The relatively high magnetic volume fraction indicates that the ferromagnetism in this sample is not entirely due to Co clustering. With a Co concentration of only 5 %, and taking into account the contribution of stray fields to the muon signal, we would expect a much smaller magnetic volume fraction than the observed. Therefore, substitutional Co mainly contributes to the large fraction of ferromagnetic phase. This result also confirms the intrinsic nature of relevant ferromagnetic ordering in Co doped TiO₂, no matter whether there are dopant clusters or not.

To understand the underlying mechanism of the dopant distribution and the origin of the observed ferromagnetism in Co doped TiO₂, we have performed extensive DFT calculations within the generalized gradient approximation [40], using the Vienna Ab initio Simulation Package (VASP) code [41], with an on-site Coulomb repulsion of $U=6.8 eV$ for Ti $3d$ orbitals and $U=6.5 eV$ for Co $3d$ orbitals [42]. First, we calculated the formation energy of various defects and their complexes in different charged states [43, 44] as a function of Fermi energy (from p -type to n -type growth conditions), as shown in Fig. 4(a). The interstitial Co ion, Co_{int}^{2+} , has high formation energy in the full range of Fermi energies; thus it is unlikely to play a significant role in mediating the

magnetism. A low oxygen pressure favors the formation of oxygen vacancies (V_O) and Ti interstitial (Ti_{int}). Isolated V_O is only stable in the +2 state and Ti_{int} only in the +4 state, both acting as efficient charge donors, resulting in a n -type conductivity. Both V_O^{2+} and Ti_{int}^{4+} ions are nonmagnetic, indicating that the magnetic moment is mainly from Co dopants and their complexes, which is in agreement with Ref. [45–47] and our XMCD results. Isolated substitutional Co_{Ti} is stable in the (0) and (-2) (i.e. Co^{2+} replacing Ti^{4+}) charged states.

Interestingly, isolated Co_{Ti}^0 and Co_{Ti}^{2-} induce similar moments, $0.93 \mu_B$ and $0.99 \mu_B$, respectively, compared well with our experimental results. A Co_{Ti} dopant and a nearby V_O may form a $Co_{Ti}+V_O$ complex [8], with a $(2+/0)$ transition level at $1.8 eV$. $(Co_{Ti}+V_O)^{2+}$ and $(Co_{Ti}+V_O)^0$ possess spin moment 1.89 and $0.95 \mu_B$, respectively. In the n -type limit (low O partial pressure), such a complex is energetically rather unfavorable, i.e. Co_{Ti}^{2-} and V_O^{2+} prefer to be separated. The interaction of the neutral and charged Co dopants and complexes is shown in Fig. 4(b). It is found that neutral Co_{Ti} dopants prefer to form embedded clusters as the energy increases monotonically with ion separation. This is in line with previous DFT calculations [9]. Importantly, the nearest pair- Co_{Ti} couple ferromagnetically (more stable in energy by $123 meV$ over the antiferromagnetic coupling), each possessing a moment of $0.93 \mu_B$. Three- or four- Co_{Ti} closely-packed clustering structures also couple ferromagnetically, each Co_{Ti} with a moment of approximately $0.7 \mu_B$. For both neutral and charged $Co_{Ti}+V_O$ complex, the cluster configuration is energetically favored. However, such clustering behavior is significantly suppressed when the separation of complexes is larger than 4 \AA . A further separation actually lowers the relative total energy, meaning that the driving force behind clustering is short ranged. Most strikingly, charged Co_{Ti}^{2-} ions prefer to be separated due to the strong Coulomb force, as the nearest configuration is energetically the least favorable one. Thus, two factors are identified to effectively eliminate the clustering of Co dopants; one is the presence of O vacancy and the other is the n -type carrier growth condition. Note that these two are intrinsically coupled as the O vacancy itself, as well as the Ti interstitial, is a donor. Thus, the DFT results highlight the critical role of low oxygen partial pressure in the fabrication of uniform DMS, as observed in experiments. When the film is deposited under a low oxygen partial pressure (10^{-5} and 10^{-6} torr), the substitutional Co_{Ti} is uniformly distributed and long range ferromagnetic ordering is formed via the mediation of charge carriers. This situation is described in Fig. S8(c) in the Supplemental Material. When the oxygen partial pressure is relatively high during film deposition, such as 10^{-4} torr, according to the first principles calculations, clustered substitutional Co_{Ti}^0 is formed since it has low formation energy, resulting in separated magnetic polarons (note

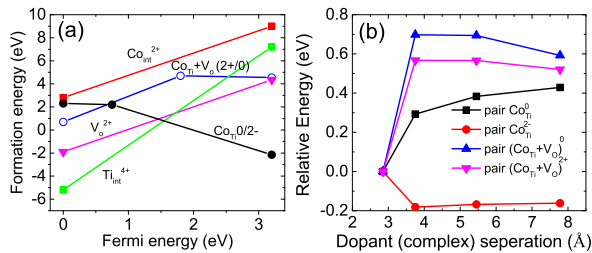


FIG. 4: (a) Calculated formation energy of the different defects in neutral and charged states in the Co-doped TiO_2 system. (b) Relative energy of neutral and charged CoTi pairs and of $\text{CoTi} + \text{V}_\text{O}$ complexes as a function of separation distance showing that charge carriers play an important role in the establishment of a uniform dopant distribution.

that this is not metallic Co clustering), which show paramagnetism at room temperature and ferromagnetism at low temperature. When the oxygen partial pressure is between 10^{-4} and 10^{-5} torr (5×10^{-5} torr), substitutional CoTi^{2-} is uniformly distributed. However, in this case the carrier concentration is too low to effectively mediate the magnetic moment to form ferromagnetic ordering. Hence, the film is paramagnetic or shows very weak ferromagnetic response. This is why the film does not have ferromagnetic phase, whereas the 10^{-4} sample has a 13% ferromagnetic phase.

In summary, using depth-resolved LE- μ SR, we find that film grown at 10^{-6} torr deposited with relatively high deposition rate is fully magnetic. The ferromagnetism is intrinsic and controlled by the oxygen vacancies. Even in the purposely prepared clustered samples, intrinsic ferromagnetic ordering mainly contributes to a large fraction of ferromagnetic phase. This work demonstrates that Co-doped TiO_2 prepared under well-controlled parameters, such as the deposition rate and oxygen partial pressure, has a uniform structure and intrinsic homogeneous ferromagnetism enforcing its position as a promising DMS candidate for spintronics devices.

Acknowledgments: H.S. and E.M. acknowledge the financial support of the MaNEP program. J.Y. acknowledges the support of the Australia Research Council discovery project Grants No. DP110105338 and No. DP140103041.

* Corresponding E-mail: elvezio.morenzoni@psi.ch

† Corresponding E-mail: jiabao.yi@unsw.edu.au

- [1] T. Dietl, H. Ohno, F. Matsukura, J. Cibert, and D. Ferrand, *Science* 287, 1019 (2000)..
- [2] Y. Matsumoto, M. Murakami, T. Shono, T. Hasegawa, T. Fukumura, M. Kawasaki, P. Ahmet, T. Chikyow, S. Koshihara, and H. Koinuma, *Science* 291, 854 (2001)..
- [3] J. Philip, A. Punnoose, B. I. Kim, K.M. Reddy, S. Layne, J. O. Holmes, B. Satpati, P. R. LeClair, T. S. Santos, and

- J. S. Moodera, *Nat. Mater.* 5, 298 (2006)..
- [4] Y. Yamada, K. Ueno, T. Fukumura, H. T. Yuan, H. Shimotani, Y. Iwasa, L. Gu, S. Tsukimoto, Y. Ikuhara, and M. Kawasaki, *Science* 332, 1065 (2011)..
- [5] H. Pan, J. B. Yi, L. Shen, R. Q. Wu, J. H. Yang, J. Y. Lin, Y. P. Feng, J. Ding, L. H. Van, and J. H. Yin, *Phys. Rev. Lett.* 99, 127201 (2007)..
- [6] J. B. Yi, C. C. Lim, G. Z. Xing, H.M. Fan, L. H. Van, S. L. Huang, K. S. Yang, X. L. Huang, X. B. Qin, B. Y. Wang, T. Wu, L. Wang, H. T. Zhang, X. Y. Gao, T. Liu, A. T. S. Wee, Y. P. Feng, and J. Ding, *Phys. Rev. Lett.* 104, 137201 (2010).
- [7] H. Ohno, *Science*, **281**, 951 (1998).
- [8] H. Ohno, D. Chiba, F. Matsukura, T. Omiya, E. Abe, T. Dietl, Y. Ohno, and K. Ohtani, *Nature (London)* 404, 390 (2000).
- [9] A. Ney, K. Ollefs, S. Ye, T. Kammermeier, V. Ney, T. C. Kaspar, S. A. Chambers, F. Wilhelm, and A. Rogalev, *Phys. Rev. Lett.* 100, 157201 (2008).
- [10] T. C. Kaspar, T. Droubay, S.M. Heald, P. Nachimuthu, C.M.Wang, V. Shutthanandan, C.A. Johnson, D. R. Gamelin, and S.A. Chambers, *New J. Phys.* 10, 055010 (2008).
- [11] J.-Y. Kim, J. H. Park, B. G. Park, H. J. Noh, S. J. Oh, J. S. Yang, D. H. Kim, S. D. Bu, T.W. Noh, H. J. Lin, H. H. Hsieh, and C. T. Chen, *Phys. Rev. Lett.* 90, 017401 (2003).
- [12] T. Dietl and H. Ohno, *Rev. Mod. Phys.* **86**, 187 (2014).
- [13] K. Sato, L. Bergqvist, J. Kudrnovsk, P. H. Dederichs, O. Eriksson, I. Turek, B. Sanyal, G. Bouzerar, H. Katayama-Yoshida, V. A. Dinh, T. Fukushima, H. Kizaki, and R. Zeller, *Rev. Mod. Phys.* 82, 1633 (2010).
- [14] S. R. Shinde, S. B. Ogale, J. S. Higgins, H. Zheng, A. J. Millis, V. N. Kulkarni, R. Ramesh, R. L. Greene, and T. Venkatesan, *Phys. Rev. Lett.* 92, 166601 (2004).
- [15] S. A. Chambers, T. Droubay, C.M. Wang, A. S. Lea, R. F. C. Farrow, L. Folks, V. Deline, and S. Anders, *Appl. Phys. Lett.* 82, 1257 (2003).
- [16] E. Morenzoni, T. Prokscha, A. Suter, H. Luetkens, and R. Khasanov, *J. Phys. Condens. Matter* 16, S4583 (2004).
- [17] See Supplemental Material which includes Refs. [18-25], for details of the thin film fabrication and characterization, of the μ SR measurements and fitting as well as of the first principle calculations.
- [18] E. Morenzoni, H. Gluckler, T. Prokscha, H. P. Weber, E.M. Forgan, T. J. Jackson, H. Luetkens, Ch. Niedermayer, M. Pleines, M. Birke, A. Hofer, J. Litterst, T. Riseman, G. Schatz, *Physica B(Amsterdam)* 289, 653 (2000).
- [19] T. Prokscha, E. Morenzoni, K. Deiters, F. Foroughi, D. George, R. Kobler, A. Suter, and V. Vrankovic, *Nuclear Instrum. Methods Phys. Res., Sect. A* 595, 317 (2008).
- [20] E. Morenzoni, F. Kottmann, D. Maden, B. Matthias, M. Meyberg, Th. Prokscha, Th. Wutzke, and U. Zimmermann, *Phys. Rev. Lett.* 72, 2793 (1994).
- [21] D. Eckstein, *Computer Simulation of Ion-Solid Interactions* (Springer, Berlin, Heidelberg, New York, 1991).
- [22] E. Morenzoni, H. Glckler, T. Prokscha, R. Khasanov, H. Luetkens, M. Birke, E.M. Forgan, Ch. Niedermayer, and M. Pleines, *Nuclear Instrum. Methods Phys. Res., Sect. B* 192, 433 254 (2002).
- [23] A. Suter and B.M. Wojek, *Phys. Procedia* 30, 69 (2012).
- [24] V. I. Anisimov, J. Zaanen, and O. K. Andersen, *Phys. Rev. B* 44, 943 (1991).

- [25] G. Kresse and D. Joubert, Phys. Rev. B **59**, 1758 (1999).
- [26] B.T. Thole, P. Carra, F. Sette, and G. van der Laan, Phys. Rev. Lett. **68**, 1943 (1992).
- [27] V. R. Singh, K. Ishigami, V. K. Verma, G. Shibata, Y. Yamazaki, T. Kataoka, A. Fujimori, F.-H. Chang, D.-J. Huang, H.-J. Lin, C. T. Chen, Y. Yamada, T. Fukumura, and M. Kawasaki, Appl. Phys. Lett. **100**, 242404 (2012).
- [28] Y. Du, Y. Zhu, S. Xi, P. Yang, H. O. Moser, M. B. H. Breese, and A. Borgna, J. Synchrotron Radiat. **22**, 839 (2015).
- [29] A. Yaouanc and P. Dalmas de Réotier *Muon Spin Rotation, Relaxation and Resonance*, International Series of Monographs on Physics Vol. 147 (Oxford University Press, Oxford, 2011).
- [30] S. R. Dunsiger, J. P. Carlo, T. Goko, G. Nieuwenhuys, T. Prokscha, A. Suter, E. Morenzoni, D. Chiba, Y. Nishitani, T. Tanikawa, F. Matsukura, H. Ohno, J. Ohe, S. Maekawa, and Y. J. Uemura, Nat. Mater. **9**, 299 (2010).
- [31] A. V. Boris, Y. Matiks, E. Benckiser, A. Frano, P. Popovich, 456 V. Hinkov, P. Wochner, M. Castro-Colin, E. Detemple, V. K. Malik, C. Bernhard, T. Prokscha, A. Suter, Z. Salman, E. Morenzoni, G. Cristiani, H.-U. Habermeier, and B. Keimer, Science **332**, 937 (2011).
- [32] E. Morenzoni, B.M. Wojek, A. Suter, T. Prokscha, G. Logvenov, and I. Boovi, Nat. Commun. **2**, 272 (2011).
- [33] H. Saadaoui, Z. Salman, H. Luetkens, T. Prokscha, A. Suter, W. A. MacFarlane, Y. Jiang, K. Jin, R. L. Greene, E. Morenzoni, and R. F. Kiefl, Nat. Commun. **6**, 6041 (2015).
- [34] A. Suter, E. Morenzoni, T. Prokscha, B. M. Wojek, H. Luetkens, G. Nieuwenhuys, A. Gozar, G. Logvenov, and I. Boovi, Phys. Rev. Lett. **106**, 237003 (2011).
- [35] J. M. D. Coey, M. Venkatesan, and C. B. Fitzgerald, Nat. Mater. **4**, 173 (2005).
- [36] E. Morenzoni, H. Glckler, T. Prokscha, R. Khasanov, H. Luetkens, M. Birke, E.M. Forgan, Ch. Niedermayer, and M. Pleines, Nuclear Instrum. Methods Phys. Res., Sect. B **192**, 254 (2002).
- [37] S. D. Yoon, Y. Chen, A. Yang, T. L. Goodrich, X. Zuo, K. Ziemer, C. Vittoria, and V. G. Harris, J. Magn. Magn. Mater. **309**, 171 (2007).
- [38] M. Weissmann, V. Ferrari, and A. Sal, J. Mater. Sci. **45**, 4945 (2010).
- [39] K. A. Griffin, A. B. Pakhomov, C.M. Wang, S.M. Heald, 479 and K.M. Krishnan, Phys. Rev. Lett. **97**, 157204 (2005).
- [40] J. P. Perdew, K. Burke, and M. Ernzerhof, Phys. Rev. Lett. **77**, 3865 (1996)
- [41] G. Kresse and D. Joubert, Computat. Mater. Sci. **6**, 15 (1996).
- [42] V. I. Anisimov, J. Zaanen, and O. K. Andersen, Phys. Rev. B **44**, 943 (1991).
- [43] C. G. Van de Walle and J. Neugebauer, J. Appl. Phys. **95**, 3851 (2004).
- [44] X. Y. Cui, B. Delley, A. J. Freeman and C. Stampfl, Phys. Rev. B **76**, 045201 (2007).
- [45] H.M. Weng, X.P. Yang, J.M. Dong, H. Mizuseki, M. Kawasaki and Y. Kawazoe, Phys. Rev. B **69**, 125219 (2004).
- [46] Z. Yang, G. Liu, and R. Wu, Phys. Rev. B **67**, 060402 (2003).
- [47] H. Kizaki, M. Toyoda, K. Sato, and H. Katayama-Yoshida, Applied Physics Express **2**, 053004 (2009).